Modeling the Influence of Nozzle-Generated Turbulence on Diesel Sprays

G. M. Magnotti*[1], K. E. Matusik[2], D. J. Duke[2], B. W. Knox[1], G. L. Martinez[1], C.F. Powell[2], A. L. Kastengren[3], C. L. Genzale[1]

[1] Woodruff School of Mechanical Engineering, Georgia Institute of Technology, Atlanta, GA 30332
[2] Energy Systems Division, Argonne National Laboratory, Lemont, IL 60439
[3] X-Ray Science Division, Argonne National Laboratory, Lemont, IL 60439

Abstract

The physical mechanisms governing spray breakup in direct injection engines, such as aerodynamic-induced instabilities and nozzle-generated cavitation and turbulence, are not well understood due to the experimental and computational limitations in resolving these processes. Recent x-ray and visible extinction measurements have been conducted with a targeted interest in the spray formation region in order to characterize the distribution of droplet sizes throughout the spray. Detailed analysis of these measurements shows promise of yielding insight into likely mechanisms governing atomization, which can inform the improvement of spray models for engine computational fluid dynamic (CFD) codes.

In order to investigate potential atomization mechanisms, we employ a joint experimental and computational approach to characterize the structure of the spray formation region using the Engine Combustion Network Spray D injector. X-ray tomography, radiography and ultra-small angle x-ray scattering measurements conducted at the Advanced Photon Source at Argonne National Laboratory quantify the injector geometry, liquid fuel mass and Sauter mean diameter (SMD) distributions under non-vaporizing conditions. Diffused back-illumination imaging measurements, conducted at the Georgia Institute of Technology, characterize the asymmetry of the spray structure. The selected range of injection pressures (50 – 150 MPa) and ambient densities (1.2 – 22.8 kg/m^3) allow for the influence of aerodynamic forces on the spray to be studied in a controlled and systematic manner, while isolating the atomization process from the effects of vaporization. In comparison to high ambient density conditions, the spray is observed to be more asymmetric at low ambient density conditions. Although several mechanisms may cause asymmetries in the nozzle exit flow conditions and ultimately the spray distribution, irregularities in the internal nozzle geometry were identified, suggesting an increased sensitivity of the spray structure to internal nozzle surface finish imperfections at such conditions. The presence of these asymmetries may influence the ability to interpret line-of-sight measurements and their derived SMD values and trends from a single viewing angle of the spray. With this consideration in mind, the measured local sensitivities to ambient density suggest that for ambient densities less than 2.4 kg/m^3, aerodynamic effects are likely suppressed, allowing the influence of turbulent-induced breakup to be isolated. In concert with the experimental measurements, we utilize three-dimensional, CFD Lagrangian-Eulerian spray simulations in CONVERGE to evaluate the details of the predicted spray structure. In particular, we compare measured and predicted sensitivities of the SMD distribution to changes in injection and ambient conditions from three different atomization models, namely Kelvin Helmholtz (KH), KH Aerodynamics Cavitation Turbulence (KH-ACT), and the newly developed KH-Faeth hybrid model. While none of the existing hybrid spray models were able to replicate the experimentally observed sensitivities, it was found that the scales characterizing the KH-Faeth model show promise of capturing the experimentally observed trends if the effects of secondary droplet breakup are neglected. These results inform recommendations for future experiments and computational studies that can guide the development of an improved spray breakup model.

*Corresponding author: gina.magnotti@gatech.edu

INTRODUCTION

To meet stringent regulations and reduction in consumption of fossil fuels, predictive computational design tools are needed to accelerate the development of cleaner burning and more fuel efficient engines. Recent advances in low temperature combustion strategies have sought methods to simultaneously reduce soot and NOx emissions. By and large, low temperature combustion concepts utilize fuel injections early in the cycle during the compression stroke, between 20-40 crank angle degrees before top dead center, to control fuel-air mixing prior to ignition while in-cylinder temperatures are still low [1-4]. Continuation of existing computational studies [3-4] could help optimize the use of direct injection an effective control strategy. However, one of the greatest barriers to predictive engine simulations is the uncertainty in representing the physics linking flows within the injector and the resultant injection and spray formation process. In order to guide design and control improvements over conventional diesel operation, it is necessary to have models that are capable of faithfully representing the physics of spray formation for a wide range of ambient density and injection pressure conditions.

To date, the capability of existing models to accurately predict spray structure details, such as droplet size, has not been exhaustively assessed at engine-relevant conditions. For conventional diesel operating conditions, aerodynamic spray breakup has been shown to adequately represent the measurable spray quantities for the non-cavitating Spray A injector [5-6]. However, work by Faeth et al. has shown that the influence of aerodynamic forces on the spray breakup process is suppressed when the liquid-to-gas density ratio (ρ_f / ρ_g) is increased above 500 [7]. For n-dodecane at room temperature, this proposed transition would occur for ambient densities less than 2.0 kg/m^3. Controlled experimental studies under such conditions would enable the physics of turbulence-induced breakup to be studied in isolation, and allow for the characterization of length and time scales that should be incorporated into a turbulent spray breakup model.

For ambient densities less than 2.0 kg/m^3, we expect the influence of aerodynamic breakup to be suppressed due to the reduced inertia of the ambient gas. Therefore, internal nozzle flow phenomena are expected to more strongly impact the resultant spray structure. Previous computational studies from Magnotti and Genzale have explored different scalings for turbulent atomization mechanisms and their influence on the spray structure in the central and peripheral regions of the spray [5]. To date, the ability of these turbulent atomization models to characterize spray breakup under low ambient density conditions has not been directly validated to date. As a result, much work is still needed to assess existing models, and develop improved formulations that are capable of faithfully representing these physics and their influence on the predicted spray structure, particularly for injection into relatively low ambient density environments.

This work highlights our findings while characterizing the resultant spray structure at conditions relevant to low temperature combustion strategies. In particular, we focus our attention on conditions where the effects due to aerodynamic instabilities can be suppressed, and ideally where turbulent breakup can be isolated. A suite of experimental techniques are employed to characterize the injector geometry, nozzle exit flow conditions, and spray characteristics for the Engine Combustion Network (ECN) Spray D injector. We first assess the ability of characterizing the spray structure from a single viewing angle by evaluating the spray asymmetry exhibited in diffused back-illumination (DBI) images. With this information in mind, ultra-small angle x-ray scattering (USAXS) measurements of Sauter mean diameter (SMD) along the spray centerline are used to evaluate the experimentally observed sensitivities to changes in injection and ambient conditions. These local sensitivities are then compared with modeling predictions from three different spray breakup models, as previously reported in a computational study by Magnotti and Genzale [5]. In particular, we evaluate the ability of the Kelvin Helmholtz (KH), KH Aerodynamic Cavitation Turbulence (KH-ACT), and KH-Faeth spray breakup models to represent the experimentally observed responses to changes in injection and ambient conditions. These findings are used to inform future experimental and computational work to further understand the influence of internal nozzle flow conditions on the spray breakup process, and how these physics should be best represented in a spray model.

EXPERIMENTAL CHARACTERIZATION OF DIESEL INJECTOR AND SPRAY PARAMETERS

Experimental and simulated conditions used in this work to study the spray structure of non-vaporizing diesel sprays are detailed in Table 1. The ECN Spray D injector nozzle #209133 is utilized in this work, which features a single-orifice diesel injector with a nominal diameter of 180 μm, available to all participants of the ECN [8]. Discussion of the experimental data sets can be found below. It should be noted that all experimental measurements are conducted during the steady portion of the spray event, when the injector needle is fully lifted and the injection velocity has reached a nominally constant value.

Table 1. A summary of experimental conditions for the Engine Combustion Network Spray D injector [8] measured and modeled in this work. The total injected mass, injection duration and nozzle discharge coefficient are given for an injection pressure of 50 MPa and an ambient pressure of 2 MPa from [5].

Experimental Parameter	**Spray D #209133**		
Nozzle Outlet Diameter [μm]	186		
Nozzle Discharge Coefficient (C_d)	0.90		
Injection Duration [ms]	4.69		
Total Injected Mass [mg]	51.6		
Fuel	n-dodecane		
Fuel Temperature [K]	303		
Ambient Temperature [K]	303		
Ambient Composition	100% N_2		
Ambient Pressure (P_{amb}) [MPa]	2	0.2	0.1
Density Ratio (ρ_f / ρ_g)	32.7	310.4	620.8
Fuel Injection Pressure [MPa]	50	150	

X-Ray Tomography of ECN Spray D

Injector nozzle tomography measurements were performed at the 7-BM beamline at the Argonne Advanced Photon Source (APS) [9]. These measurements utilized x-ray images of the injector nozzle from 1800 lines of sight and computed tomography to reconstruct the geometry of the internal flow passages. A detailed description of the procedure can be found in [10]. The final geometry has a spatial resolution of 1.8 μm, allowing nozzle features to be determined with great precision. Key features from the computed tomography are compared to nominal manufacturer's specifications, as shown in Table 2. Although the actual nozzle outlet diameter is reasonable close to the nominal specification, the manufacturing process resulted in a more cylindrical nozzle orifice profile than specified, as indicated by the smaller measured K-factor,

$$K = \frac{d_{inlet} - d_{outlet}}{10} \quad (1)$$

where the nozzle orifice inlet and outlet diameters, d_{inlet} and d_{outlet}, respectively, are defined in microns.

Table 2. Comparison of ECN Spray D 209133 injector nozzle geometry dimensions with manufacturer's specifications.

	Nozzle Outlet Diameter [μm]	***K***	***Mean Inlet Radius of Curvature [μm]***
Nominal Specifications [8]	180	1.5	--
ECN Spray D 209133 [10]	186 ± 2	0.8	207 ± 4

Characterization of Nozzle Exit Flow Conditions

The rate-of-injection (ROI) profile for the Spray D nozzle, as shown at the reference condition of P_{amb} of 2 MPa and P_{inj} of 150 MPa in Figure 1, is used to define the injection velocity boundary condition in the spray simulations. Details regarding the nozzle flow coefficients and total injected mass are detailed in Table 1. The Spray D ROI profile was obtained from rate-of-momentum measurements conducted in the Georgia Institute of Technology's (Georgia Tech) spray combustion chamber using the impingement technique for ECN nozzle #209133, along with measurements of total collected mass over 50 injections. Details regarding the experimental measurement technique, uncertainty quantification, and spray vessel can be found in previous work performed at Georgia Tech [11-13].

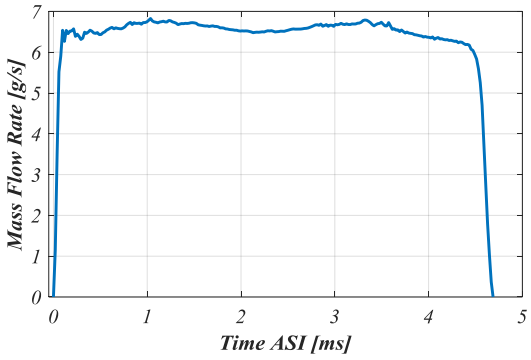

Figure 1. Spray D measured rate of injection from [5] at P_{amb} = 2 MPa and P_{inj} = 50 MPa.

Diffused Back-Illumination Imaging

In order to characterize the spray structure and boundary, diffused back-illumination (DBI) imaging measurements were performed in a continuous-flow optically-accessible high-temperature, high-pressure spray chamber at Georgia Tech. This spray chamber is capable of creating a quasi-quiescent environment with air, 99.5% N_2, or any mixture of the two at a maximum temperature and pressure of 950 K and 10 MPa. All of the experiments for this study were conducted with air at room temperature. There exists approximately 100 mm of optical access at the front, sides, and the top of the chamber. The spray chamber was designed by Advanced Combustion Gmbh and is similar to other continuous flow-through spray chambers in the literature [14].

Line-of-sight, 2D extinction maps of the spray were developed by utilizing a diffused back-illumination arrangement following the recommendations of Westlye et al [15], as shown in Figure 2. The resulting image resolution for the optical arrangement was approximately 78 µm/pixel. To freeze the motion of the spray, a Light-Speed Technologies white LED was used with a pulse width of 90 ns. A Photron SA-X2 camera, fitted with a 50-mm f/1.2 les, captured the spray at 72 kfps while the LED pulsed every other frame. The camera captured a dark frame every other frame, which allowed the sensor to reset prior to the next frame. Westlye et al. recommended this procedure as a way to reduce error in the measured extinction due to ghosting, which is residual charge left on the sensor for the next frame [15].

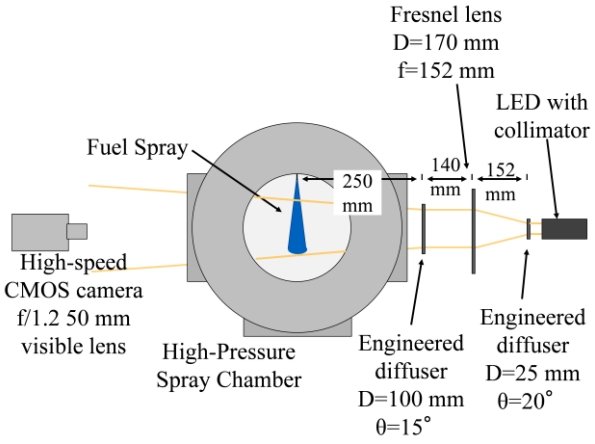

Figure 2. Experimental arrangement for diffused back-illuminated imaging.

X-Ray Radiography

X-ray radiography and ultra-small angle x-ray scattering (USAXS) measurements were performed on Spray D at the Advanced Photon Source (APS) at Argonne. During both measurements, the Spray D injector was horizontally mounted in a pressure chamber fitted with a pair of 12 × 30 mm x-ray transparent windows. The chamber was pressurized to the desired back pressure with N_2, which was also used to maintain a continuous purge flow of approximately 4 standard L min^{-1} through the chamber to minimize droplet formation on the windows during data acquisition. A diesel common-rail injection system was used to pressurize n-dodecane fuel to the desired rail pressure. The injector was fired at 3 Hz for a commanded injection duration of 2.0 ms.

Detailed descriptions of the time-resolved radiography measurements may be found in previous work [9, 16-18]. In brief, a monochromatic beam at 8 keV energy passed through a set of curved mirrors which focused the beam to a 5 × 6 µm point. The incoming beam intensity, I_0, was measured using a diamond x-ray beam monitor placed upstream of the pressure chamber. The outgoing beam intensity, I, downstream of the pressure chamber was measured with a PIN diode. As the x-ray beam passed through the fuel spray, photons were absorbed through the process of photoelectric absorption, attenuating the beam by an amount related to the quantity of fuel in the beam path. From the change in beam intensity, the pathlength, l, of fuel in the beam path can be determined with the Beer-Lambert law,

$$l = \frac{1}{\mu\rho_f}\log\left[\frac{I_0}{I}\right], \qquad (2)$$

where ρ_f and μ are the density and attenuation coefficient of the fuel, respectively. Between 16 and 32 spray events were averaged at each measurement point, and the x-ray beam was raster scanned in both the axial and transverse coordinates to create an ensemble-averaged map of the line-of-sight pathlength of fuel.

Ultra-Small Angle X-Ray Scattering

USAXS measurements were performed at the 9-ID beamline of the APS in order to characterize the total surface area per sample volume of the spray. By combining the surface area measured with USAXS and the density measured with radiography, the SMD, or d_{32}, of the droplet size distribution can be determined. The SMD is defined as

$$d_{32} = 6\frac{V}{A}, \qquad (3)$$

where V and A are the volume and surface area of a group of particles, respectively.

Data were recorded in a 1 ms interval during the steady-state portion of the spray event. Background measurements were also recorded over 80 ms before each scan to account for any changes within the measurement domain caused by previous spray events. The 9-ID beamline is equipped with a Bonse-Hart instru-

ment to measure the scattering intensity, $I_{scat}(q)$, as a function of scattering vector, q [19]. A schematic of the experiment set-up is shown in Figure 3.

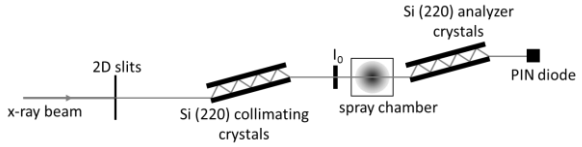

Figure 3. Schematic of the USAXS experiment.

A beam of x-rays at 21 keV was first shaped into a 50 × 500 μm H × V spot by a set of high precision 2D slits. The beam was then collimated using a pair of Si (220) crystals before impinging on the spray. As the beam passed through the spray, x-rays were scattered at small angles. The scattered x-rays were filtered downstream with a pair of Si (220) analyzer crystals, and the resulting intensity measured with a detector. The pair of analyzer crystals were rotated to vary q between 1×10^{-4} Å^{-1} < q < 1×10^{-2} Å^{-1} with a step size of 1×10^{-5} Å^{-1} at low q, with increasing step size for larger q. The scattered beam intensity as a function of q was measured at axial distances ranging from 1 to 20 mm downstream of the injection nozzle tip, at the centerline of the spray. Once $I_{scat}(q)$ is measured, post-processing is performed using the Irena data analysis package [20] in order to obtain the surface area per volume of fuel droplets.

In order to find the spray centerline during USAXS measurements, a transverse scan at fixed q was also recorded at each axial location of interest. The spray centerline was taken to be the transverse location at which the beam intensity was a maximum, i.e. the location with the highest droplet density. Radiography measurements were temporally averaged during the steady portion of the spray event for the SMD calculation. The transverse profiles from the USAXS and radiography measurements were each centered about their full width at half maximum in order to index the profiles onto the same coordinate system. Because the transverse location of the USAXS measurement is known at each axial distance, the corresponding radiography data at that location may be found. The USAXS measurement point is assumed to be in the center of the 50 × 500 μm window. All measured radiography points that fall within this window are averaged to arrive at one value of the pathlength, with interpolation and appropriate weighted averaging performed to accurately incorporate the edges of the window. The pathlength of fuel obtained from the radiography measurements provides the line-of-sight integrated volume of droplets in a sample of unit thickness. The USAXS measurements provide the line-of-sight surface area per volume of droplets, likewise in a sample of unit thickness. Thus, the two measurements can be combined per Equation 3 to arrive at a line-of-sight integrated SMD value at each measured axial location.

COMPUTATIONAL SPRAY MODELING

Aerodynamically-induced and turbulent-induced primary spray breakup were modeled to evaluate the local sensitivity of the central SMD distribution to changes in ambient and injection conditions, particularly for injection into relatively low ambient density environments. These modeling predictions were shown in previous work by Magnotti and Genzale [5]. The CFD model set-up has been described in previous work by the authors [5, 21], but the salient details of the spray model are discussed below.

CFD Code

The commercial CFD code, CONVERGE [22], was employed to model the injection of an n-dodecane spray into a constant volume chamber. The measured fuel mass flow rate, shown in Figure 1, and nozzle discharge coefficient, listed in Table 1 [5], were used to calculate the injection velocities at the nozzle exit. Liquid mass is injected within a circle instead of at a point source to yield better mass distribution in the near-nozzle region [23]. The radius of the circle is equal to the nozzle radius. Using the "blob" injection model [24], 1 million computational parcels were injected to represent the dense spray. Primary spray breakup was modeled with either the KH model [25], the hybrid KH-ACT model [26], or the KH-Faeth model [5]. The KH-Faeth model is a new hybrid aerodynamic-turbulence model recently developed by Magnotti and Genzale, and introduced in [5]. Secondary droplet breakup was modeled using the KH model [25]. Other implemented sub-models include the standard k-ε turbulence model [27] with a turbulent round-jet correction [28] to represent the flow in the gaseous ambient environment. It should be noted that the effects of cavitation were not considered in this computational study in order to evaluate the ability of turbulent spray breakup alone to match the experimentally observed sensitivities to changes in injection and ambient conditions.

Computational Mesh and Initial Conditions

The spray chamber was modeled using a three-dimensional hexahedral structured mesh, as shown in Figure 4. A large domain was selected in order to model a free fuel jet, where the wall effects are insignificant within the timescales and regions of interest. Fixed embedding was employed in the near-nozzle region to resolve the flow near the injector, with a minimum cell size of 125 μm. Using two levels of Adaptive Mesh Refinement (AMR), the grid was further refined outside of this region for the velocity field to yield a grid with a maximum of 1.7 million cells. A grid convergence study was presented in previous work by the authors

[21] to justify the selection of the grid. Computations were initialized with a uniform ambient quiescent charge in the spray chamber. The aerodynamic component of the spray breakup models (KH) was calibrated to match the centerline SMD USAXS measurements performed on the ECN Spray A injector [29], as detailed in [5-6].

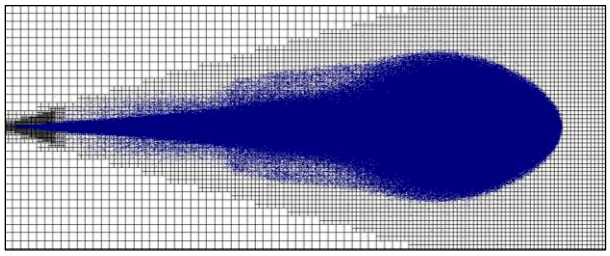

Figure 4. Instantaneous slice of the computational mesh of constant volume spray chamber at the spray centerline at t = 1.0 ms ASI. The 3-D mesh is composed of a maximum of 1.7 million cells, with a minimum cell size of 125 μm in the near-nozzle region.

RESULTS AND DISCUSSION

In this work, we compare the measured and predicted sensitivities of the centerline SMD distributions to changes in injection and ambient conditions. These results help identify in order to identify current modeling inaccuracies and inform a directed path towards improving the physical underpinnings of spray breakup models. We first assess the ability to characterize the spray structure from a single measurement viewing angle by evaluating the spray asymmetry exhibited in diffused back-illumination images. With this information in mind, USAXS measurements of SMD along the spray centerline are used to evaluate the experimentally observed sensitivity to changes in injection and ambient conditions. These local sensitivities are then compared with the hybrid spray breakup modeling predictions. These findings are used to inform future experimental and computational work to further understand the influence of internal nozzle flow conditions on the spray breakup process, and how these physics should be best represented in a spray model.

Spray D Injector Nozzle Geometry

Computed X-ray tomography measurements enable detailed characterization of the internal nozzle geometry. Comparison of the internal nozzle profiles of two ECN Spray D injectors, #209133 and #209134 are shown in Figure 5(a). The two injectors are observed to have identical *K*-factors of 0.8 and identical nozzle outlet diameters of 186 μm, within the range of experimental uncertainty. Although differences can be seen in the internal nozzle geometry in the sac volume of the two injectors, these differences are not expected to appreciably change the internal nozzle flow conditions during the steady portion of injection when the needle is fully lifted. As a result, it is expected that both of these injectors would produce similar sprays.

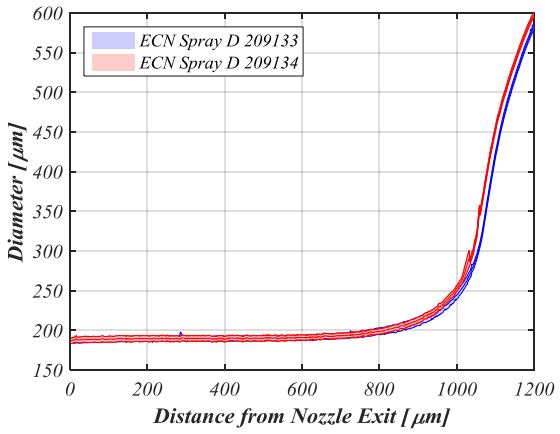

(a)

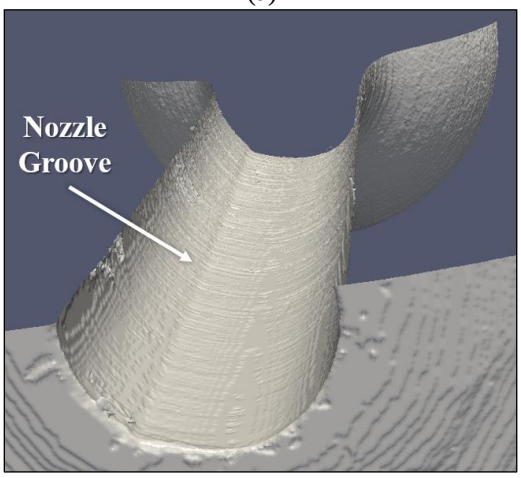

(b)

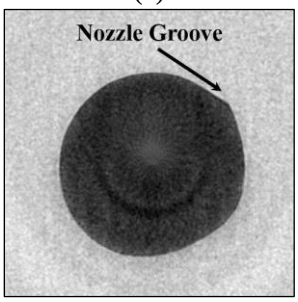

(c)

Figure 5. Detailed internal nozzle geometry measurements from x-ray tomography conducted at the APS [10]. (a) Comparison of geometries for two ECN Spray D injectors, where the nozzle orifice outlet is located on the left hand side of the plot. Cross-section of the (b) iso-surface of Spray D #209133 and (c) nozzle hole are shown.

Further evaluation of the reconstructed internal nozzle geometry of the Spray D #209133 injector used in this work, as shown in Figure 5(b), reveals unique features in the nozzle orifice. In particular, a groove can be seen that runs along the length of the nozzle orifice, and results in an eccentric nozzle outlet profile, as shown in Figure 5(c). If conditions exist where the resultant spray is sensitive to asymmetries in the internal nozzle geometry, this could result in different spray structures between the two injectors. Additionally, spray asymmetries could influence the ability to characterize the spray structure using projected line-of-sight measurements from a single viewing angle. Evaluation of the DBI measurements can help identify conditions where the spray may be sensitive to these features in the internal nozzle geometry, and where the approximation of symmetry is valid for characterizing the spray structure.

Influence of Ambient and Injection Conditions on Spray Asymmetry

Using the DBI measurements, we first examine our implicit assumption of symmetry when utilizing a single viewing angle of the spray to characterize the spray structure, and identify potential limits on the applicability of this approximation. Figure 6(a)-(b) show examples of time-averaged 2D extinction maps produced for P_{inj} of 50 MPa and P_{amb} conditions of 2 MPa and 0.1 MPa, respectively, with the injector nozzle centered at 0-mm in the axial and transverse coordinates. In general, high levels of optical thickness can be seen along the spray centerline, which has been shown to correlate with high droplet number densities [30]. With increasing radial distance from the spray centerline, the spray becomes more diffuse and the optical thickness decreases. Evaluation of the 2D extinction maps reveals that the spray appears more asymmetric at the lower P_{amb} condition shown in Figure 6(b) in comparison to the higher P_{amb} condition shown in Figure 6(a). This trend is likely due to enhanced entrainment and local mixing, which would diffuse the appearance of asymmetric features. These results suggest that asymmetries and surface imperfections within the internal nozzle geometry may have a more noticeable influence on the global spray distribution as the ambient environment approaches atmospheric conditions.

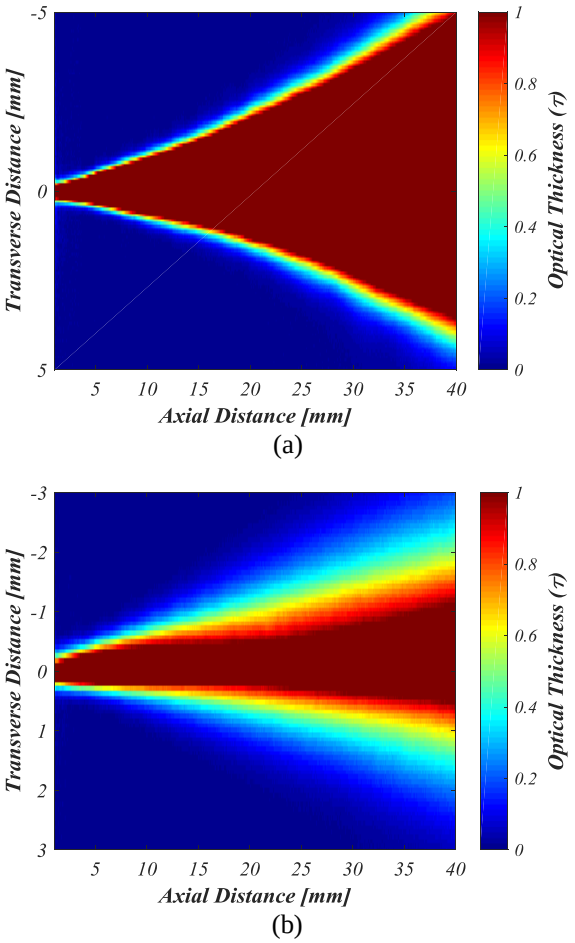

Figure 6. Example 2D extinction map obtained from DBI measurements are shown for P_{inj} of 50 MPa and P_{amb} of (a) 2 MPa and (b) 0.1 MPa.

To quantitatively characterize the influence of injection and ambient conditions on the asymmetry of the spray, as observed in the DBI measurements in Figure 6, transverse distributions of the optical thickness, $\tau(y)$, are evaluated. As shown in Figure 7(a), $\tau(y)$ at a distance of 12 mm from the nozzle exit is compared for two back pressure conditions (0.1 MPa and 2 MPa), and two injection pressures (50 MPa and 150 MPa). Consistent with the observations from Figure 6, the transverse optical thickness distributions are more asymmetric for P_{amb} conditions less than 0.2 MPa. To quantify the degree of asymmetry at a given location in the spray for a given condition, $\tau(y)$ is first decomposed into its symmetric and asymmetric components, $\tau^{+}(y)$ and $\tau^{-}(y)$, respectively, as mathematically defined below:

$$\tau(y) = \tau^{+}(y) + \tau^{-}(y) \quad (4)$$

$$\tau^{+}(y) = \frac{1}{2}\{\tau(y) + \tau(-y)\} \quad (5)$$

$$\tau^{-}(y) = \frac{1}{2}\{\tau(y) - \tau(-y)\} \quad (6)$$

where y is the transverse position at a fixed axial location, x, in the spray. The l^2–norm, $||\tau^+||_2$ and $||\tau^-||_2$, can then be used to quantify the magnitude of $\tau^+(y)$ and $\tau^-(y)$. Employing these definitions, the symmetry of τ, $S(\tau)$, can be quantified as follows,

$$S(\tau) = \frac{\|\tau^+(y)\|_2}{\|\tau^+(y)\|_2 + \|\tau^-(y)\|_2} \quad (7)$$

where S =1 indicates a symmetric distribution and S = 0 indicates a perfectly asymmetric distribution.

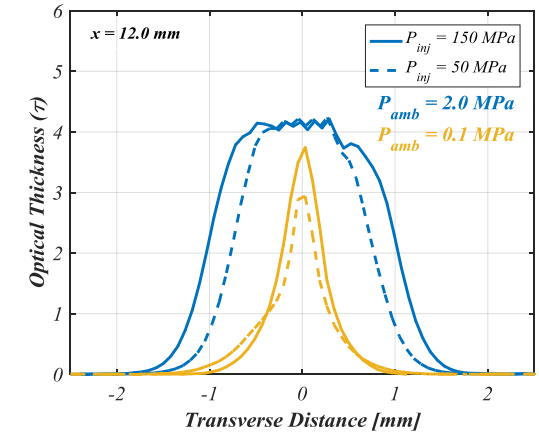

(a)

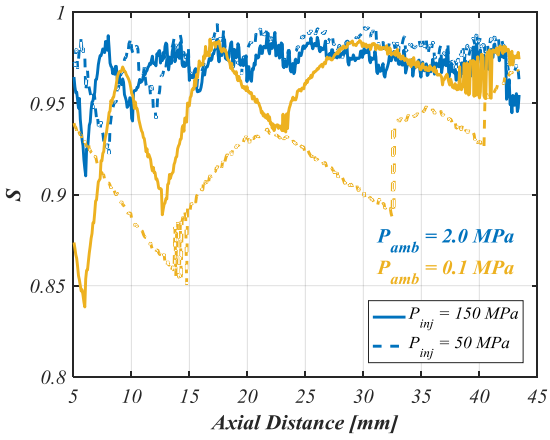

(b)

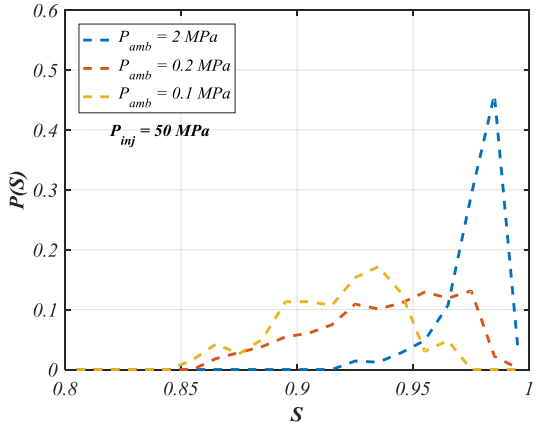

(c)

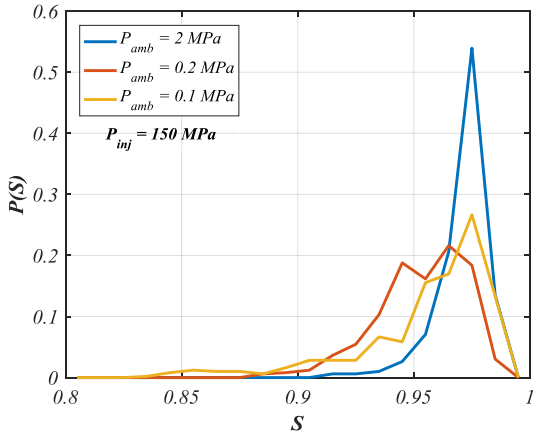

(d)

Figure 7. Example transverse distributions of the optical thickness from DBI measurements at a distance of 12 mm from the nozzle exit are shown in (a). The symmetry factor, S, is quantified for each axial slice in the spray and plotted in (b). Probability distributions of S throughout the spray are shown for P_{inj} of (c) 50 MPa and (d) 150 MPa.

The degree of asymmetry observed in the DBI measurements can now be quantified throughout the spray for a given condition by evaluating the axial distribution of $S(\tau(y))$, as shown in Figure 7(b). For P_{amb} condition of 2 MPa, some variation in S is observed throughout the spray. However, the spray structure, as indicated by the optical thickness, is generally symmetric ($S \approx 0.98$). These features are more clearly visualized in the histograms in Figure 7(c)-(d) for the P_{amb} condition of 2 MPa and P_{inj} conditions of 50 and 150 MPa. The peak probability of S, $P(S)$, occurs at approximately S = 0.98. The probability distributions are also seen to be quite narrow, indicating that the approximation of spray symmetry is valid throughout the spray.

However, for P_{amb} conditions of 0.1 MPa and 0.2 MPa, the distributions appear more asymmetric with greater variability throughout the spray, as shown in

Figure 7(b)-(d). As shown in Figure 7(c), for the back pressure condition of 0.1 MPa and injection pressure of 50 MPa, the most probable S throughout the optical thickness distribution ($S \approx 0.92$) is less than the highest P_{amb} condition. Additionally, the spread of $P(S)$ is observed to be much wider, indicating more variable degrees of asymmetry throughout the spray. At the P_{inj} condition of 150 MPa as shown in Figure 7(d), the most probable S for an ambient condition of 0.1 MPa is similar to that observed for the higher P_{amb} condition ($S \approx 0.98$). However, the variability of S throughout the spray is observed to be much higher.

These results indicate that as the back pressure is decreased and approaches atmospheric conditions (0.1 MPa), the assumption of spray symmetry may not be appropriate at many locations throughout the spray. As previously noted, this asymmetry may be due to geometrically asymmetric features within the nozzle, as shown in Figure 5. These results suggest potential consequences on the line-of-sight measurements and the resultant SMD. A single viewing angle may not be able to adequately characterize the mean projected quantities and average SMD along the spray centerline. Therefore, the SMD quantities and their experimentally observed responses to changes in injection and ambient conditions should be interpreted with these potential uncharacterized effects in mind.

Influence of Injection and Ambient Conditions on the Resultant Centerline SMD

USAXS measurements of SMD along the spray centerline for Spray D #209133 are shown in Figure 8, along with curve fitted to the data to illustrate the general trends in droplet size evolution. In general, the measured SMD decreases with increasing axial distance from the nozzle exit, indicating continual breakup of the spray and droplets. The SMD along the spray centerline is also seen to increase with decreasing P_{amb} and P_{inj}. However, the experimental measurements suggest a transition in droplet formation behavior as ρ_f / ρ_g increases beyond 100, which corresponds to P_{amb} less than or equal to 0.2 MPa. For ρ_f / ρ_g greater than 500, Faeth et al. have shown that aerodynamic forces do not exert a significant influence on the droplet formation process [7]. The similarity in SMD distributions from the USAXS measurements for P_{inj} of 50 MPa and P_{amb} of 0.1 and 0.2 MPa conditions suggests that changing the aerodynamic inertia by a factor of two does not appreciably change the droplet formation process. However, for P_{inj} of150 MPa, a larger change in SMD is observed when P_{amb} is increased from 0.1 to 0.2 MPa.

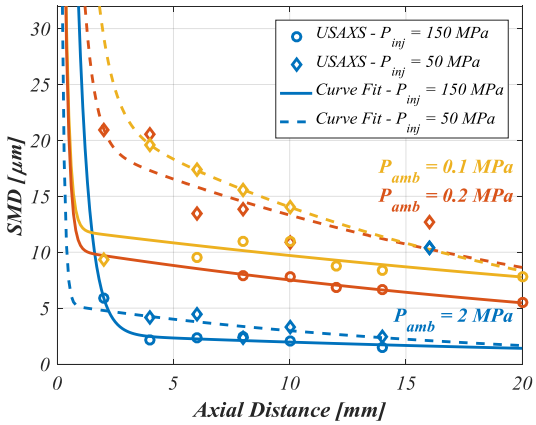

Figure 8. SMD measurements from x-ray measurements conducted at the APS are shown for a range of ambient and injection conditions along the spray centerline. A two-term exponential function is fit to the data (solid and dashed lines).

In order to extract more detailed information about the local sensitivity of the SMD to changes in injection and ambient conditions, the axial distribution of SMD is fit to a two-term exponential function for each condition. The curve fit is of the form

$$f(x) = Ae^{Bx} + Ce^{Dx} \tag{8}$$

where A, B, C, and D are unique fitting parameters for each condition. An additional point of 186 μm at the nozzle exit ($x = 0$) was added to each data set to capture the rapid decrease in SMD from its initial value of the nozzle outlet diameter. The two-term exponential function captures the data well, with an R^2-value greater than 0.99 for all conditions.

Using these curve fits, the local sensitivity of SMD to changes in injection and ambient conditions can be quantified. The local sensitivities to changes in P_{inj}, $S_{P_{inj}}$, and P_{amb}, $S_{P_{amb}}$, are defined as follows:

$$S_{P_{inj}} = \frac{SMD(P_{inj} = 150\ MPa, P_{amb}, x = x_i)}{SMD(P_{inj} = 50\ MPa, P_{amb}, x = x_i)} \tag{9}$$

$$S_{P_{amb}} = \frac{SMD(P_{inj}, P_{amb} = 0.2\ MPa, x = x_i)}{SMD(P_{inj}, P_{amb} = 0.1\ MPa, x = x_i)} \tag{10}$$

$S_{P_{inj}}$ and $S_{P_{amb}}$ characterize the relative decrease in SMD as P_{inj} or P_{amb} is increased at a particular axial distance, x_i, from the nozzle exit. S_i equal to unity indicates that the centerline SMD is relatively insensitive to changes in parameter i, assuming all other parameters are held constant. Similarly, S_i approaching zero indicates that the centerline SMD is highly sensitive to changes in parameter i.

The local sensitivities for the USAXS measurements of centerline SMD to changes in P_{inj} and P_{amb} are shown in Figure 9 for x_i = 10 mm. Indeed, these results confirm previous qualitative observations. At a fixed P_{inj} of 50 MPa, the SMD is not strongly influenced by the change in P_{amb} from 0.1 to 0.2 MPa, as indicated by the high $S_{P_{amb}}$ value of 0.95. The strongest sensitivity of centerline SMD is observed with respect to changes in P_{inj} at P_{amb} of 0.2 MPa. It should be noted that the reported sensitivities are relatively constant regardless of the x_i selected within the range of the experimental measurement locations.

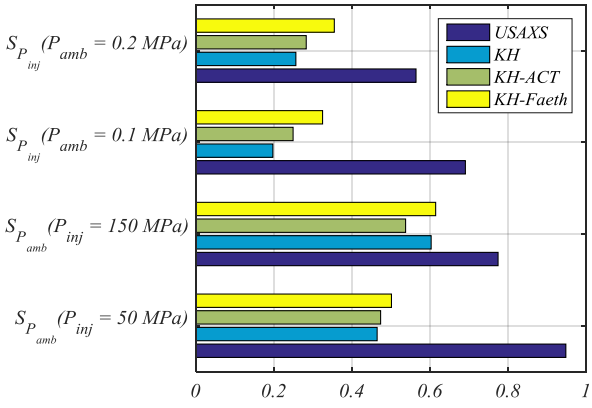

Figure 9. Local sensitivities to changes in P_{inj} and P_{amb} for ρ_f / ρ_g conditions greater than 300, as indicated by the x-ray measurements and evaluated spray breakup models.

Evaluation of Turbulent Breakup Model Spray Predictions

Using the previously published droplet size predictions for the KH, KH-ACT and KH-Faeth spray models [5], the ability of different atomization models to capture the experimentally observed trends can be evaluated. Instead of focusing on the ability of well-calibrated models to quantitatively match the experimental measurements, we compare the sensitivities of measured and predicted SMD to changes in injection and ambient conditions. To allow for direct comparison with the USAXS measurements, we evaluate the sensitivity of the predicted minimum SMD along the spray centerline [5], SMD_{min}, to changes in injection and ambient conditions, as shown in Figure 9.

Comparison between the predicted and measured sensitivities of the centerline SMD distribution to changes in injection and ambient conditions reveals several discrepancies. Predicted $S_{P_{amb}}$ by each model at a fixed P_{inj} indicates a stronger influence of P_{amb} on the centerline SMD than is observed experimentally. Additionally, all spray breakup models exhibit larger sensitivities to P_{inj}, and therefore smaller $S_{P_{inj}}$, than is indicated by the USAXS measurements.

As noted in previous work by Magnotti and Genzale [5], in the absence of droplet interactions, predicted droplet sizes within the central region of the spray are determined through a competition between the primary atomization and secondary droplet breakup length scales. All evaluated spray models employ an identical KH secondary droplet breakup model. Droplets that are larger than the wavelength of the fastest growing KH surface wave, Λ_{KH}, are unstable to KH instabilities and subsequently breakup. For ρ_f / ρ_g greater than 100, the KH, KH-ACT and KH-Faeth primary atomization models produced droplets that were larger than Λ_{KH}, and underwent subsequent droplet breakup. As a result, for low ambient density conditions, the SMD_{min} predicted by each of the models was strongly influenced by the secondary droplet breakup process, and the predicted sensitivities were observed to scale with the KH mechanism representing the droplet breakup [5]. This finding is confirmed by the similar $S_{P_{inj}}$ and $S_{P_{amb}}$ predicted by the KH and hybrid spray breakup models, as shown in Figure 9. Therefore, comparison between the predicted and measured sensitivities reveals that the experimentally measured SMD along the spray centerline are not well represented by either the KH primary atomization or secondary droplet breakup models under low ambient density conditions (ρ_f / ρ_g greater than 300).

Although the influence of the secondary droplet breakup model obfuscates the sensitivities of the turbulence-induced primary atomization models at low ambient density conditions, analysis of the length scales governing these models can provide clearer insight. In the KH-ACT model [26], the resultant droplet size is assumed to scale with the integral length scale. The resultant droplet size scales with the dimension of the flow, and is independent of the Reynolds number and ambient environment properties [31]. As a result, the theoretical droplet size is insensitive to changes in P_{inj} and P_{amb}, which would yield $S_{P_{inj}}$ and $S_{P_{amb}}$ equal to 1.0. These results suggest smaller predicted sensitivities with respect to changes in the injection and ambient conditions than is observed in the USAXS SMD measurements in Figure 9. Therefore, the centerline distribution of SMD is not likely well represented by the KH-ACT primary atomization model [26], or any turbulent breakup model that assumes that the resultant droplets are proportional in size to the integral length scale [32-33].

The assumed scaling of turbulence-induced breakup in the KH-Faeth model exhibits different sensitivities to changes in injection and ambient conditions. Based on their analysis of the measured liquid surface ligament and droplet properties at the onset of turbulent breakup from holographic imaging, Wu and Faeth de-

veloped an empirical correlation to relate the resultant droplet size to nozzle exit turbulence properties [7]. The empirical correlation is employed in the KH-Faeth model [5] to represent the resultant droplet size, L_{Faeth}, and is reproduced below:

$$\frac{L_{Faeth}}{\Lambda} = C_{sx}\left(\frac{x}{\Lambda We_{f\Lambda}^{1/2}}\right)^{2/3} \qquad (11)$$

where Λ is the radial integral length scale, C_{sx} is an empirical constant set to 0.65, x is the axial position where droplets are formed, $We_{f\Lambda}$ is the Λ-based liquid Weber number ($\rho_f U_{inj}^2 \Lambda/\sigma$), U_{inj} is the injection velocity, and σ is the surface tension of the liquid. By estimating U_{inj} using the Bernoulli equation, a relationship among L_{Faeth}, P_{inj} and P_{amb} can be approximated:

$$L_{Faeth} \propto We_{f\Lambda}^{-\frac{1}{3}} \propto U_{inj}^{-\frac{2}{3}} \propto \left(P_{inj} - P_{amb}\right)^{-\frac{1}{3}} \qquad (12)$$

Using the relation in Equation (12), $S_{P_{inj}}$ and $S_{P_{amb}}$ can be calculated to characterize the response of the KH-Faeth turbulence-induced primary atomization model to changes in injection and ambient conditions. For a fixed P_{inj} of 50 MPa or 150 MPa, $S_{P_{amb}}$ is approximately equal to 1.0, suggesting a larger insensitivity of the centerline SMD to changes in P_{amb} than is indicated by the measurements in Figure 9. However, a three-fold increase in P_{inj} at a fixed P_{amb} of 0.1 MPa or 0.2 MPa results in $S_{P_{inj}}$ of approximately 0.69. Comparison with $S_{P_{inj}}$ of the USAXS measurements, as shown in Figure 9, reveals improved agreement between the measured and predicted sensitivities. Although the estimated $S_{P_{amb}}$ and $S_{P_{inj}}$ show some small discrepancies with the experimentally observed sensitivities, it is important to consider potential uncertainty in the measured SMD sensitivity. In particular, as previously noted, spray asymmetries exhibited at low P_{amb} conditions may influence the ability to characterize the mean projected quantities and average SMD along the spray centerline from a single viewing angle. Discrepancies in the predicted and measured sensitivities may be due to the uncharacterized influence of asymmetries in the spray distribution on the centerline SMD. It is therefore possible for a properly calibrated KH-Faeth spray model that neglects the effects of secondary droplet breakup to well characterize the experimentally observed sensitivities of SMD to changes in injection and ambient conditions.

Further experimental characterization of the internal nozzle flow conditions through the use of x-ray fluorescence [34-35] and phase contrast imaging [35-36] could provide more detailed information on the influence of internal nozzle geometry imperfections on the asymmetry of exit flow conditions and ultimately on the spray structure. Additionally, because the spray is observed to be more asymmetric at low P_{amb} conditions, additional viewing angles should be evaluated in the experimental measurements to characterize the azimuthal distribution of SMD at the spray centerline. Tomographic reconstruction of the projected measurements could help characterize the three dimensional distribution of droplet sizes in the spray. Future computational studies can assess the ability of a calibrated KH-Faeth spray model to capture the experimentally observed trends in the USAXS measurements when secondary droplet breakup is neglected.

CONCLUSIONS

Future high-efficiency clean combustion engines will very likely employ fuel injection strategies over a wide portion of the cycle in order to control emissions formation in-cylinder. Simulation-based design of these fuel injection strategies will require robust spray models that can deliver predictive trends over a wide range of in-cylinder and injection conditions. To support the development of such spray models, experimental measurements of Spray D #209133 were performed to characterize the injector geometry, exit flow conditions, and resultant spray structure. The influence of changing injection and ambient conditions on the predicted droplet size distribution from existing spray breakup models, namely the Kelvin-Helmholtz model based on aerodynamic-induced breakup of the spray into droplets, and two hybrid spray breakup models, the KH-ACT and KH-Faeth models, which consider the competing effects of aerodynamics and nozzle-generated turbulence on the spray breakup process, were evaluated. Analysis of experimental measurements and comparison with aerodynamically-induced and hybrid spray breakup model predictions of the centerline droplet size distribution revealed the following:

1. Two-dimensional extinction maps from temporally averaged diffused back-illumination images indicated increased asymmetry in the overall spray structure at low back pressure conditions. Quantification of symmetry, S, in the extinction distribution throughout the spray revealed that sprays injected into high back pressure conditions of 2 MPa were found to be consistently symmetric, regardless of injection pressure. For injection into low back pressure conditions less than 0.2 MPa, the spray was found to have greater variation in S throughout the spray.
2. Asymmetric flow conditions at the injector nozzle exit likely explain the observed asymmetries in the spray distribution. Irregularities in the internal nozzle geometry was investigat-

ed as a potential contributing factor. Computed x-ray tomography exposed a groove along the length of the nozzle orifice and an eccentric nozzle outlet profile. The experimental evidence suggests that the increased variation in spray symmetry at low back pressure conditions may be linked to asymmetry in the nozzle geometry.

3. USAXS measurements suggest that a change in spray breakup behavior occurs between the 2 MPa and 0.2 MPa back pressure conditions. Two-term exponential functions were fit to each centerline distribution of SMD to allow for quantification of the local sensitivity of SMD to changes in injection and ambient conditions. Under conditions where the influence of ambient gas inertia is expected to be sufficiently suppressed, the SMD along the spray centerline was seen to strongly vary with injection pressure, and less so with ambient density.
4. Comparison between measured and predicted sensitivities of the centerline SMD to changes in injection and ambient conditions revealed that none of the evaluated hybrid spray models were able to replicate the experimentally observed sensitivities. These discrepancies were found to be largely due to the strong influence of the KH secondary droplet breakup sub-model on the model predictions. However, it was found that the turbulence-induced breakup length scale characterizing the KH-Faeth model shows promise of capturing the experimentally observed sensitivities if the effects of secondary droplet breakup are neglected. Future computational studies can evaluate the ability of a calibrated KH-Faeth model to capture the experimentally observed centerline SMD distribution and sensitivities to changes in injection and ambient conditions.

Further experimental and computational work is required to characterize the potential influence of internal nozzle geometric features on the internal flow and exit conditions, particularly for injection into low ambient density environments. X-ray fluorescence and phase contrast imaging could provide more detailed information on the internal nozzle phenomena. Additionally, because the spray is observed to be more asymmetric at low P_{amb} conditions, additional viewing angles should be evaluated in the experimental measurements to characterize the azimuthal distribution of SMD at the spray centerline.

ACKNOWLEDGMENTS

This material is based upon work supported by the Department of Energy, Office of Energy Efficiency and Renewable Energy (EERE) and the Department of Defense, Tank and Automotive Research, Development, and Engineering Center (TARDEC), under Award Number DE-EE0007333.

We gratefully acknowledge the computing resources provided on Blues, a high-performance cluster operated by the Laboratory Computing Resource Center at Argonne National Laboratory. Use of the Advanced Photon Source is supported by the U.S. Department of Energy under Contract No. DEAC02-06CH11357.

The authors would like to thank Mr. Yoontak Kim for helping with the measurements for the rate of momentum, total injected mass and nozzle flow coefficients for the Engine Combustion Network Spray D #209133 injector.

NOMENCLATURE

APS	Advanced Photon Source
C_d	Discharge coefficient
DBI	Diffused back-illumination
ECN	Engine Combustion Network
KH	Kelvin-Helmholtz
KH-ACT	Kelvin-Helmholtz Aerodynamic-Cavitation-Turbulence
P_{amb}	Ambient back pressure
P_{inj}	Injection pressure
ROI	Rate of injection
SMD	Sauter mean diameter
S	Symmetry factor
$S_{P_{amb}}$	Local sensitivity of SMD to changes in P_{amb} at a fixed P_{inj}
$S_{P_{inj}}$	Local sensitivity of SMD to changes in P_{inj} at a fixed P_{amb}
USAXS	Ultra-small angle X-ray scattering

REFERENCES

1. Pickett, L., Kook, S., and Williams, T., "Transient Liquid Penetration of Early-Injection Diesel Sprays," *SAE Int. J. Engines* 2(1):785-804, 2009.
2. Kolodziej, C., Kodavasal, J., Ciatti, S., Som, S. et al., "Achieving Stable Engine Operation of Gasoline Compression Ignition Using 87 AKI Gasoline Down to Idle," *SAE Technical Paper* 2015-01-0832, 2015.
3. Kodavasal, J., et al., "CFD Simulation of Gasoline Compression Ignition," *ASME Internal Combustion Engine Division Fall Technical Conference*, Columbus, IN, 2014.
4. Kodavasal, J., Pei, Y., Harms, K., Ciatti, S. et al., "Global Sensitivity Analysis of a Gasoline Compression Ignition Engine Simulation with Multiple Targets on an IBM Blue Gene/Q Supercomputer," *SAE Technical Paper* 2016-01-0602, 2016.
5. Magnotti, G.M. and Genzale, C.L., *SAE Technical Paper* 2017-01-0829, 2017.

6. Magnotti, G.M. and Genzale, C.L., *Int. J. Multiphase Flows*, Submitted.
7. Wu, P.-K., and Faeth, G.M., *Atomization and Sprays*, 3:265-289, 1993.
8. Engine Combustion Network, "Engine Combustion Network: Injector Spray D Nozzle Geometry," https://ecn.sandia.gov, accessed March 2017.
9. A. Kastengren, C.F. Powell, D. Arms, E.M. Dufresne, H. Gibson, and J. Wang., *J Synchrotron Rad*, 19:654-657, 2012.
10. Matusik, K.E., Duke, D.J., Swantek, A.B., Powell, C.F., and Kastengren, A.L., "High resolution x-ray tomography of injection nozzles," *ILASS-Americas 28th Annual Conference on Liquid Atomization and Spray Systems*, 2016.
11. Knox, B.W., Franze, M.J., Genzale, C.L., "Diesel Spray Rate-of-Momentum Measurement Uncertainties and Diagnostic Considerations," ASME J. Eng. Gas Turbines Power, 138(3): 2016.
12. Falcone, J.A., Knox, B.W., and Genzale, C.L., "Identifying Uncertainties in Diesel Spray Rate-of-Momentum Transients Under Elevated Back Pressure," ASME 2015 Internal Combustion Engine Division Fall Technical Conference, Houston, Texas, 2015.
13. Knox, B.W., and Genzale, C.L., "Effects of End-of-Injection Transients on Combustion Recession in Diesel Sprays," SAE Int. J. Engines, 9(2): 932-949, 2016.
14. Meijer, Maarten, Bart Somers, Jaclyn Johnson, Jeffrey Naber, Seong-Young Lee, Louis Marie Malbec, Gilles Bruneaux et al. *Atomization and Sprays*, 2012.
15. Westlye, F.R., Penney, K., Skeen, S., Manin, J., Pickett, L. and Ivarsson, A., *Applied Optics*, 2016, *Submitted*.
16. Kastengren, A.L., Powell, C.F., Riedel T., Cheong, S.-K., Im, K.-S., Liu, X. Wang, Y.J., and Wang, J. , *J. Fluid. Eng.*, 130:0413-01-12, doi: 10.1115/1.2903516.
17. Kastengren, A. L., Tilocco, F., Duke, D. J., Powell, C., Zhang, X., and Moon, S., "Time-Resolved X-Ray Radiography of Sprays from Engine Combustion Network Spray A Diesel Injectors," *Atomization and Sprays*, 24(3), 251–272, 2014.
18. Kastengren, A., and Powell, C. F. "Synchrotron X-ray techniques for fluid dynamics," *Experiments in Fluids*, 55(3), 1686, 2014.
19. Ilavsky, J., Jemian, P. R., Allen, A. J., Zhang, F. et al., *J. Appl. Cryst.*, 42(3):469-479, 2009.
20. Ilavsky, J. and Jemian, P. R., *J. Appl. Cryst.*, 42(2):347–353, 2009.
21. Magnotti, G.M., and Genzale, C.L., *SAE Int. J. Fuels Lubr.*, 8(1):167-178, 2015.
22. Richards, K.J., Senecal, P.K., Pomraning, E., CONVERGE™ (Version 2.1) Manual, Convergent Science Inc., 2013.
23. Senecal, P.K., Pomraning, E., Richards, K.J., Som, S., "Grid-Convergent Spray Models for Internal Combustion Engine Computational Fluid Dynamics Simulations," Journal of Energy Resources Technology, 136(1): 2013.
24. Dukowicz, J. K., *Journal of Computational Physics*, 1980.
25. Reitz, R.D., *Atomisation and Spray Technology*, 3: 309-337, 1987.
26. Som, S., Ramirez, A.I., Aggarwal, S.K., Kastengren, A.L. et al., *SAE Technical Paper* 2009-01-0838, 2009.
27. Han, Z., and Reitz, R.D., *Comb. Sci. Tech*., 106:267-295, 1995.
28. Pope, S., *AIAA Journal*, 16:279-281, 1978.
29. Kastengren, A., Ilavsky, J., Viera, J.P., Payri, R., Duke, D.J., Swantek, A., Tilocco, F.Z., Sovis, N., and Powell, C.F., *Int. J. Multiphase Flows*, In Press.
30. Magnotti, G.M., and Genzale, C.L., *Atomization and Sprays*, 5:397-424, 2015.
31. Pope, S.B., "Turbulent Flows," (Cambridge University Press, 2000).
32. Huh, K.Y., and Gosman, A.D., "A phenomenological model of diesel spray atomization," *Proceedings of the International Conference of Multi-Phase Flows*, Tsukuba, Japan, 1991.
33. Huh, K.Y., Lee, E., and Koo, J., "Diesel Spray Atomization Model Considering Nozzle Exit Turbulence Conditions," *Atomization and Sprays*, 8(4): 453-469, 1998.
34. Duke, D.J., Swantek, A.B., Sovis, N., Powell, C.F., Kastengren, A.L., and Fezzaa, K., "Recent Developments in X-ray Diagnostics for Cavitation," *SAE International Journal of Fuels and Lubricants*, 8(1):135-146, 2015.
35. Duke, D., Kastengren, A., Swantek, A., Matusik K., and Powell, C., "X-ray Fluorescence Measurements of Dissolved Gas and Cavitation," *Exp. Fluids*, 57(10):1-14, 2016.
36. Duke, D., Swantek, A., Tilocco, Z., Kastengren, A. et al., "X-ray Imaging of Cavitation in Diesel Injectors," *SAE Int. J. Engines*, 7(2):1003-1016, 2014.